

**Improvement of orbit determination using laser altimeter crossovers
JUICE mission case study**

Villamil, S.; Dirkx, D.; Stark, A.; Hussmann, H.

DOI

[10.1016/j.actaastro.2021.02.005](https://doi.org/10.1016/j.actaastro.2021.02.005)

Publication date

2021

Document Version

Final published version

Published in

Acta Astronautica

Citation (APA)

Villamil, S., Dirkx, D., Stark, A., & Hussmann, H. (2021). Improvement of orbit determination using laser altimeter crossovers: JUICE mission case study. *Acta Astronautica*, 182, 587-598.
<https://doi.org/10.1016/j.actaastro.2021.02.005>

Important note

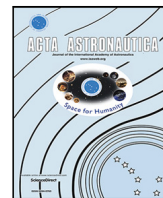
To cite this publication, please use the final published version (if applicable).
Please check the document version above.

Copyright

Other than for strictly personal use, it is not permitted to download, forward or distribute the text or part of it, without the consent of the author(s) and/or copyright holder(s), unless the work is under an open content license such as Creative Commons.

Takedown policy

Please contact us and provide details if you believe this document breaches copyrights.
We will remove access to the work immediately and investigate your claim.



Research paper



Improvement of orbit determination using laser altimeter crossovers: JUICE mission case study

S. Villamil^{a,b,c,*}, D. Dirkx^c, A. Stark^b, H. Hussmann^b

^a DLR (German Aerospace Center) Society for Space Applications (GfR) mbH, Münchener Str. 20, 82234 Wessling, Germany

^b German Aerospace Center (DLR), Institute of Planetary Research, Rutherfordstraße 2, 12489 Berlin, Germany

^c Delft University of Technology (TU Delft), Kluyverweg 1, 2629 HS Delft, Netherlands

ARTICLE INFO

Keywords:

Orbit determination
 Altimetry crossovers
 Laser altimetry
 JUICE mission

ABSTRACT

This work evaluates the added benefit of using laser altimeter measurements for orbit reconstruction. As a spacecraft orbits a celestial body, its altimetry swaths progressively cross previous swaths. These locations, known as crossover points, yield valuable information about the orbited body and the spacecraft trajectory. The mathematical expressions for the inclusion of crossover measurements into orbit determination algorithms are presented and evaluated. It is shown that a first-order approximation of these expressions is insufficient and a more detailed expression is developed. To evaluate the impact of altimetry crossover measurements on orbit determination, the planetary mission Jupiter Icy moons Explorer (JUICE) by the European Space Agency (ESA) is used as a case study by means of a covariance analysis. In this initial analysis, the assumption is made that all altimetry measurements are obtained with nadir pointing which limits the direct applicability of our method until pointing is accounted for.

1. Introduction

The JUICE mission has been selected by the European Space Agency (ESA) as the first L-class mission within its Cosmic Vision Program 2015–2025 with its main goal being the study and further characterisation of the Galilean satellites, in particular Ganymede [1].

The JUICE mission aims to build upon previous observations and missions, such as the Galileo mission launched by the National Aeronautics and Space Administration (NASA) [2]. Of those results, the strong evidence for subsurface oceans within Jupiter's icy moons is particularly revolutionary as the existence of liquid water drastically increases the potential for the moons' habitability. Thus, a deeper understanding of the Jovian system would not only provide insights into the formation of gas giants and their satellites, but also into the conditions for habitability within icy moons. Further remarkable results from previous efforts include insights into the Jovian system atmospheres and magnetospheres, in particular Ganymede's internal magnetic field [3–8].

For precise orbit reconstruction the on-board radio science instrument 3GM (Gravity and Geophysics of Jupiter and the Galilean Moons) is included on JUICE. By using range and range-rate (Doppler) measurements, 3GM also aims to constrain Ganymede's interior structure

by determining its gravity field, tidal Love number k_2 and rotational variations [9].

The JUICE mission is also equipped with the GALA (Ganymede Laser Altimeter) instrument. Its functioning is based on the principle of two-way laser ranging, with its primary task being the determination of the Jovian moons' topography. GALA will also measure Ganymede's tidal deformation to infer knowledge about its internal structure and rheology, in particular through determination of its h_2 Love number [10]. Additionally, it will contribute to constraining Ganymede's rotational state [11]. GALA is expected to witness radial surface deformations on Ganymede of up to 7 metres due to Jupiter's tidal forcing, assuming a typical value of 1.3 for the Love number h_2 [12]. Additionally, GALA is capable to infer data from the backscattered laser pulses such as surface roughness, slope and albedo at its wavelength of 1064 nm.

Laser altimetry data allows for the construction of so-called crossover points, where altimetry arcs cross one another. At a crossover point, the altitude difference of the spacecraft during the two arcs, as measured by the instrument, can be constructed. This crossover observable can be used for the determination of the body's tidal deformation [13], as well as for contributing to the orbit determination of the spacecraft [14–17], since it encodes information on the relative state of the spacecraft at two epochs.

* Correspondence to: Münchener Str. 20, 82234 Wessling, Germany.

E-mail addresses: Sebastian.Villamil@dlr-gfr.com (S. Villamil), D.Dirckx@tudelft.nl (D. Dirkx), Alexander.Stark@dlr.de (A. Stark), Hauke.Hussmann@dlr.de (H. Hussmann).

<https://doi.org/10.1016/j.actaastro.2021.02.005>

Received 12 May 2020; Received in revised form 31 January 2021; Accepted 4 February 2021

Available online 11 February 2021

0094-5765/© 2021 Published by Elsevier Ltd on behalf of IAA.

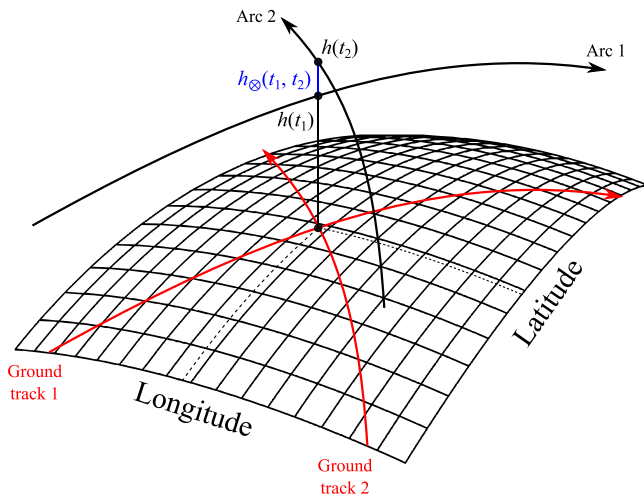


Fig. 1. Schematic of altimeter crossover geometry with nadir pointing.

In this article, we provide a description of our estimation model and the associated partial derivatives to incorporate the altimetry crossover observables into the orbit determination process, with the calculation of the individual arc partial derivatives being independent of their corresponding second arc, unless the crossover times occur during the same arc. We apply this method to a simulation of the JUICE mission, and analyse the potential contributions that this data type could have for the mission and spacecraft missions in general.

2. Altimetry crossovers

An altimetry crossover point refers to the location on a body's surface where an altimetry measurement swath crosses another swath in the body-fixed frame of the orbited body. At these locations, the crossover observable h_{\otimes} can be obtained which is the altimetry measurement difference between both altimetry swaths, with t_2 and t_1 being the crossover times on the respective swath, as shown in Eq. (1) and Fig. 1.

$$h_{\otimes}(t_2, t_1) = h(t_2) - h(t_1) = h_{\otimes 2} - h_{\otimes 1}. \quad (1)$$

If the altimeter's pointing is strictly nadir, the altimetry swaths coincide with the spacecraft's ground tracks. Under this assumption, the altimeter measurements coincide with the spacecraft's altitude difference at the crossover times. In the scope of this study, we make use of the assumption of nadir pointing. It is expected that altimetry swaths are off-nadir up to 25 m as discussed further in Section 5 which results in the altimetry footprint at least partly coinciding with the spacecraft's ground track as discussed further in Section 3.1. We discuss the implications and limitations of this assumptions further in Sections 5–7. The fact that the body-fixed latitude and longitude of the altimetry swaths are equal at the crossover times t_1 and t_2 is particularly useful as their difference in measurements h_{\otimes} yields information about the dynamical behaviour of the orbited body, such as the Love number h_2 , as they link the body's tidal response at two different epochs [12,13,18].

Previous studies on interplanetary missions such as the Mars Global Surveyor (MGS) [14,15] and the Lunar Reconnaissance Orbiter (LRO) [16,17,19,20] have shown that the use of altimetry crossover measurements leads to significant improvements in orbit determination and attitude estimation. In addition, Earth based studies have shown that altimetry crossovers can be used to independently verify corrections for systematic pointing errors on time scales of orbital period, weeks and months [21].

For MGS, the inclusion of altimetry crossovers did not focus on using the height difference at the crossover location. Instead, their

more general approach was to minimise the distance between two ground track arcs at a crossover location using batch least-squares. These ground track arcs are described by three dimensional polynomials which trace out the measured topography and can account for pointing adjustments [14,15]. Unfortunately, their altimetry footprints were widely spaced leading to an undersampling of the terrain and to a reduction of the quality of crossover observables. Using over 24 million crossovers, the spacecraft trajectory and attitude were recovered with accuracy beyond mission specifications showing that seasonal effects can also be identified, with improved solutions when pointing was also estimated. Additionally, it was found that the inclusion of crossovers improved the solution of the Mars gravity field [22].

For LRO, the crossover implementation for orbit determination was different as its altimetry measurements were obtained using a multi-beam altimeter with its beams being aligned in an X-shape resulting in five distinct altimetry tracks [16,19]. With this setup, each LRO crossover location yields several common measuring locations, significantly increasing the number of available crossover observables. For this precise orbit determination (POD) crossover implementation, the *swath crossovers* method was used which estimates the spacecraft orbit not only from its dynamics but from geometric and topographic constraints as well. The squared differences of the altimetry observables between tracks were minimised using purely geometric constraints between altimeter measurement points. These constraints are dictated by the points' total and radial distance, with the radial distance constraint of neighbouring altimeter spots being particularly strict [19]. This method demonstrated that a large sample of mid-latitude crossovers is necessary to prevent degradation in trajectory reconstruction with the solution being overly constrained near the poles. Results using actual LRO mission data showed that the inclusion of crossovers strongly improve solutions for spacecraft trajectory, pointing, lunar body tide, and the lunar gravity field [13].

Overall, these studies found that the inclusion of crossovers is highly complex and requires high computational loads [17,20], which can be lessened by using sparse matrix techniques [15]. They also found that crossovers with shallow angles between ground-tracks are unfavourable for orbit determination due to poor information on the cross-track partials [14,15]. This issue is further exacerbated by the fact that crossovers are highly sensitive to spacecraft state changes leading not only to changes in the location of crossovers, but also to the total number of crossover locations between estimation iterations. This characteristic is unique to this measurement type which results from ground tracks no longer crossing after an orbit adjustment, as well as the emergence of entirely new crossovers. For these reasons, it is suggested to employ crossovers only after an initial orbit estimation has been obtained. For an ideal state recovery, crossovers should be evenly distributed. Conversely, truly polar orbits or truly equatorial orbits may not yield satisfactory results due to the lack of global coverage. For planetary missions, orbits with a high inclination are common to achieve global coverage leading to crossovers being most prominent at the poles. This is also the case for the case study here, with Fig. 2 showing the available crossover locations during JUICE's final mission phase, denoted GCO500 (Ganymede Circular Orbit with an altitude of 500 km).

Contrary to previous studies, our approach differs in the way we include the crossover observables into orbit estimation. While previous studies directly included the topography surrounding a crossover location, we focus on the estimated, single point of the crossover occurrence and its projected change of location (and therefore change in t_1 and t_2) after the orbit adjustment. Furthermore, we detail the specific mathematical derivation of our method, demonstrating the minimum set of derivations necessary, as well as its limitations.

To assess the influence of the crossovers on the orbit determination process, the settings of which are described in Section 4, we perform a covariance analysis. Building on this approach, we present a mathematical model in Section 5 to incorporate the crossover observable

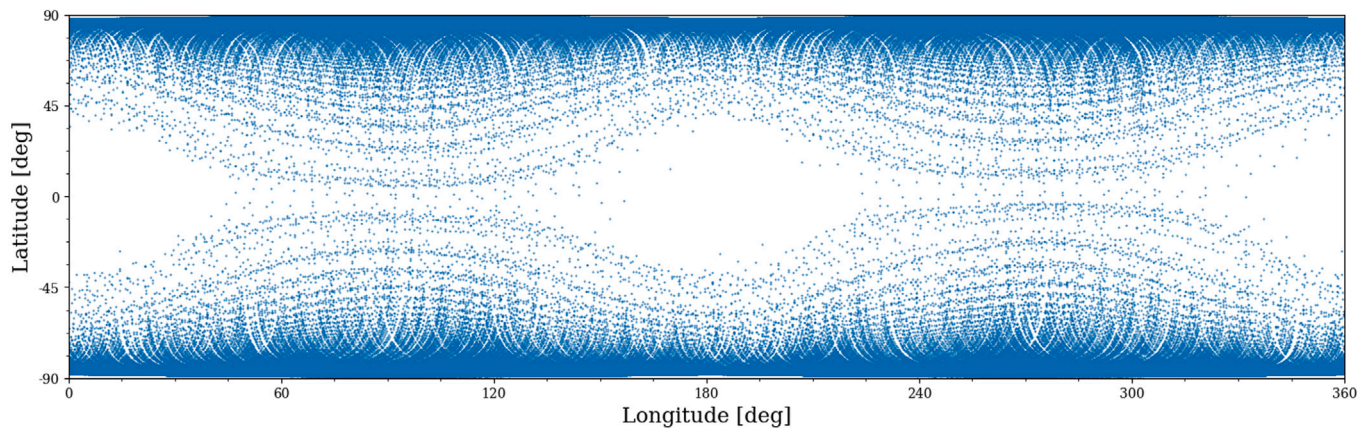


Fig. 2. Crossover locations during JUICE's GCO500 mission phase.

defined in Eq. (1) into orbit determination solutions. As discussed further in Section 6, we discuss how linking the state estimation of different estimation periods, conceptually allows improved state reconstruction during periods of low estimation quality by exploiting the direct geometrical link to periods with higher-quality estimation. Poor estimation quality can be a result of, for instance, unfavourable Doppler observation geometry or lack of line-of-sight observations to Earth.

In the remainder of this article, the assumption is made that all spacecraft altimetry measurements have nadir pointing leading them to coincide with the ground tracks. This assumption is made for better illustration and simplification of the equations. It is within our expectations that the obtained results hold in the presence of pointing.

3. Numerical simulation

Since the JUICE mission's scientific data will only be acquired in the 2030's, the analysis of its orbit determination is done with synthetic measurements obtained through numerical simulations. We consider only the mission's final phase during which JUICE is in a near-circular 500-km orbit around Ganymede, GCO500. A detailed analysis of JUICE's orbit determination from Doppler data is presented by [9]. The necessary simulations are set up using the TU Delft Astrodynamics Toolbox (Tudat) for trajectory propagation and measurement simulation [23–25]. JUICE's orbit insertion into its GCO500 orbit marks the initial epoch of our simulations with JUICE's state being estimated daily as detailed further in Section 4.2. While POD is not the goal of JUICE in GCO500, we have selected this phase as test case as it offers a large distribution of crossovers, as shown in Fig. 2, to analyse the potential contribution of crossovers to planetary missions and geodetic parameter estimation.

JUICE's nominal state in time and the relevant data of the perturbing celestial bodies are obtained from ESA's Consolidated Report on Mission Analysis (CReMA) 3.0 for the JUICE mission [26–28]. While there are later CReMA versions available, version 3.0 was chosen due to its high surface coverage which is one of the major scientific goals of GALA and other instruments. In this study, we use a multi-arc estimation with an arc length of 1 day and our dynamical model considers the following perturbations [29]:

- Galilean moons as point masses,
- Synthetic Ganymede 12×12 gravity model,
- Jupiter point mass,
- Jupiter zonal coefficient J_2 ,
- Sun point mass,
- Solar radiation pressure, spacecraft as cannonball.

For the calculation of radiation pressure a reflectivity coefficient of 1.3 is used, with an effective area of 97 m^2 and a spacecraft mass of 2000 kg [29]. The values for the other perturbations are obtained from CReMA 3.0 and are further detailed in Table A.3.

3.1. Measurement data

For the orbit reconstruction of planetary missions, the spacecraft state vector is typically estimated using almost exclusively Doppler data, as obtained by the 3GM instrument for the JUICE mission.

In this work, we do not consider the contribution of range data to JUICE's Ganymede-centred orbit determination, based on the range quality requirement of 20 cm, which is too high to contribute meaningfully to the POD, considering the exceptionally low Doppler noise, as discussed further below. Instead, range data is typically used to estimate signals with much longer periods than the spacecraft's orbit, such as the ephemerides of celestial bodies [30]. However, it should be noted that recent preliminary experiments with the MORE experiment on BepiColombo (which is very similar to 3GM of JUICE) show that the range data can have an uncertainty of only centimetres in magnitude [31,32]. If a similarly low noise level can be achieved for JUICE, the radio range data will be able to contribute to JUICE POD, in addition to the Doppler data.

A major challenge for the JUICE mission are the strong constraints regarding its measurement periods since JUICE does not have a steerable high-gain antenna for communication and data downlink. This leads to an alternation between measurement intervals and downlink periods as the entire spacecraft must be rotated to establish communication to Earth. Within this alternation, nominal tracking is only available during downlink periods which have a length of 8 h per day [29]. For a successful downlink, visibility conditions must be satisfied to establish communication, such as a minimum elevation angle of 15 degrees [9]. Finally, there must be no bodies occulting the line of sight between JUICE and the communication ground station, Malargüe (Argentina). For JUICE, the major occulting bodies to consider are Jupiter and the Sun. Lastly, all communication windows must be larger than 3.5 h.

Naturally, the frequent spacecraft rotation limits the operation of instruments which require nadir pointing, such as GALA, as they can only collect scientific measurements between tracking windows [29]. In addition to the downlink periods, the time required for the slew of the spacecraft must also be considered for the availability of GALA measurements. While slew manoeuvres are expected to require an average of 20 min, an additional 10 min must also be included for settling-in effects to subside allowing for pointing requirements to be fulfilled. Furthermore, Wheel-Off-Loading (WOL) manoeuvres must also be considered. While the final JUICE WOL procedures have not been established, current planning assumes one WOL manoeuvre before each tracking period. This choice in design aims at lowering spacecraft state and pointing uncertainties, as the effects of the WOL on the spacecraft orbit are estimated immediately after they occur. Taking a conservative approach, such a WOL manoeuvre is estimated to take up to 30 min. Unfortunately, these manoeuvres effectively reduce the average, daily available time for GALA measurements from 16 to

14.5 h. These constraints on the accumulation of altimeter measurements directly affects the number of available crossover measurements, as a crossover measurement consists of two independent altimetry measurements.

GALA takes altimetry measurements at pulse rate of 30 Hz, with the emitted laser pulse producing a surface footprint of approx. 50 m at JUICE's nominal altitude of 500 km. Together with its pulse rate, this leads to a distance of approx. 50 m between laser-spot centres and a spot-edge distance of 0 m [10].

3.2. Error sources

The 3GM instrument will use a dual-frequency (X/Ka-band) system. By combining measurements at these two frequencies, the influence of dispersive media (Earth and Jupiter ionosphere, solar plasma) can be calibrated for in the data analysis. Of the remaining non-random error sources, the noise induced by the troposphere is typically the largest [33], which can largely be modelled in the data analysis using meteorological data obtained at the ground station. Although remaining, unmodelled, error sources are not purely Gaussian, nor entirely free of systematics, past experience has shown that the data properties are quite close to these ideal conditions [33,34]. Consequently, we choose to model Doppler data noise as Gaussian uncorrelated, and do not consider Doppler biases. For 3GM, the expected Doppler precision is 3×10^{-6} m/s for an integration time of 1000 s [9]. Such high measurement precision has been proven possible by NASA's Juno mission to Jupiter which has attained a precision of 1.5×10^{-5} m/s for an integration time of 60 s, which is the Doppler measurement precision used here [33,35]. Doppler noise levels that are even lower (1.2×10^{-5} m/s) have been achieved by BepiColombo [32], and were used in the study of [9]. We retain the slightly higher value of 1.5×10^{-5} m/s, stressing that the conclusions of this work will only be weakly affected by this small reduction in Doppler noise.

For laser altimetry measurements three significant error contributors have been established: **Instrument intrinsic** errors, **pointing and alignment** errors and **interpolation** errors [12]. The determination of the magnitudes of these errors is performed using GALA's instrument requirements which define the nominal measurement conditions as: surface slope < 8 degrees, albedo > 44% and a pointing error of < 10 arcsec.

The previous missions to the Jupiter system, Voyager and Galileo, found that roughly 90% of slopes on Ganymede are between 3.5 to 8 degrees, with these slopes being on a larger scale than GALA's footprint [36]. Using these estimates, Ganymede's average global slope is approximated statistically by a surface slope of $\alpha = (3.5^\circ \times 90\% + 20^\circ \times 10\%) / 100\% = 5.15^\circ$, vastly simplifying Ganymede's surface slope to an average. Recent investigations based on Galileo data for Europa revealed that surface roughness values in specific terrains can reach high values [37]. Thus, it is possible that for Ganymede the apportionment performed above is underestimating the average surface slopes.

For this study, GALA's **instrument intrinsic** errors are assumed to be limited to a 1σ uncertainty of:

$$\Delta h_{GALA} = 0.5 \text{ m} \quad (2)$$

during JUICE's final mission phase, GCO500 [10].

Errors in **pointing and alignment** are assumed to originate from thermo-elastic distortions on GALA's optical bench, the accuracy of the star trackers, spacecraft manoeuvres and oscillations (particularly on its solar panels). We point out that the pointing error Δh_p discussed below describes the post-mission pointing uncertainty of altimetry measurements. Noticeably, this uncertainty differs from off-nadir pointing knowledge. Here, we assume strict nadir pointing, as mentioned in Section 2. For errors in pointing knowledge the assumption is made that they jitter randomly around nadir as their direction and magnitude is changed randomly after each of the frequently occurring slew manoeuvres. We make the approximation that pointing errors can

be treated as having a Gaussian distribution around nadir pointing with these errors being uncorrelated. While it can be expected that the mission's altimetry measurements will have correlations, we make the assumption that the spacecraft's daily slew manoeuvres decouple altimetry measurements after each day. This assumption is further strengthened by the vast majority of crossover measurements treated here having individual altimetry measurements at t_1 and t_2 that are more than 20 days apart. Furthermore, we point out that a persistent bias in the pointing knowledge would not produce correlated crossover observables. Each new crossover represents a new measurement of the pointing bias, independent of the measurement performed by another crossover. Even if three profiles cross exactly at the same location the correlation between two crossover observables cannot be the same. For altimetry measurements, the pointing error Δh_p can be described as a function of pointing angle error $\Delta\phi$, altitude H and surface slope α :

$$\Delta h_p = H \tan(\Delta\phi) \tan(\alpha). \quad (3)$$

While a nominal altimetry measurement of 500 km is expected during JUICE's GCO500 mission phase, rapid changes in slope due to surface features such as rims, ridges or cracks among others can strongly affect measurements. With an average surface slope of 5.15 degrees and a maximum error in pointing knowledge of 10 arcsec Eq. (3) yields 1σ pointing and alignment errors of $\Delta h_p = 2.18$ m.

Finally, the error contribution due to interpolation errors must also be considered for the calculation of the surface's height profile. Interpolation is necessary when describing the planetary surface continuously since altimeter measurements are only given at discrete epochs, making the interpolation error inherent to the measurement frequency. Taking into account GALA's measurement frequency f_q of 30 Hz, interpolation errors Δh_i can be calculated via [12]:

$$\Delta h_i = \frac{v_{surf}}{2f_q} \tan \alpha, \quad (4)$$

with v_{surf} being JUICE's velocity with respect to the surface. Approximating JUICE's GCO500 trajectory as a circular orbit to obtain its projected velocity at Ganymede's surface leads to interpolation errors with a magnitude of $\Delta h_i = 2.24$ m on average. In Eq. (4) we have assumed the worst-case, where the crossover point is exactly at the mid-point between two footprints. This is attributed to the poor knowledge on the surface and the fact that the crossover geometry is subject to changes during each iteration.

Due to the assumption that GALA's instrument, pointing and interpolation errors are independent from one another their total contribution to GALA's error budget can be calculated as:

$$\Delta h = \sqrt{\Delta h_{GALA}^2 + \Delta h_p^2 + \Delta h_i^2}. \quad (5)$$

Using Eq. (5) and the error magnitudes defined above a total altimetry measurement error budget of 3.17 m is established, with a Gaussian distribution and a mean value of zero.

The two individual altimetry measurements that make up a crossover measurement can be regarded as independent from one another due to the spacecraft rotation manoeuvres discussed above, since the second altimetry measurement is obtained at least one spacecraft orbit later in time. Thus, for a crossover measurement the error contribution of individual altimetry measurements is obtained as:

$$\Delta h_{\otimes} = \sqrt{\Delta h^2 + \Delta h^2} = \sqrt{2}\Delta h, \quad (6)$$

leading to a crossover measurement error budget of 4.48 m. For the calculation of these error budgets a conservative approach is chosen. It can be expected that for the actual measurements spacecraft pointing might be better than required and that improvements in the crossover analysis will mitigate interpolation errors.

4. Covariance analysis

4.1. Methodology

In this work, we use covariance analysis to ascertain the state and parameter uncertainty for the JUICE mission during its GCO500 orbit phase. We consider the case of Doppler-only estimation, and the case where both Doppler and altimetry crossover data is used. This work’s analysis does not aim to evaluate the ultimately attainable estimate precision for orbit determination procedures, as is done in detail by [9]. Instead, our test case is a broad analysis of the contribution of crossovers for further guidance on where to focus future efforts. Moreover, our first analysis serves as a guide on whether, and where, to focus efforts to include such high-fidelity models in future simulation studies and more importantly: in data analysis when the JUICE mission is orbiting Ganymede. This contribution is measured by analysing the covariance matrix P_x of the estimated parameters (see Section 4.2 for a list) which is defined as

$$P_x = (H^T P_y^{-1} H + \Lambda)^{-1}, \quad (7)$$

with Λ being the a priori covariance of the estimated parameters. H is the so-called *design matrix* and P_y is the measurement covariance matrix which contains the measurement uncertainties σ which determine the measurements’ weight for the parameter estimation. Assuming all measurement errors are uncorrelated and have a Gaussian distribution with zero mean, P_y is a diagonal matrix, with its elements σ_i being the uncertainty of the measurements i . Our measurement uncertainties for the Doppler and crossover observables are described in Section 3.1.

Additionally, for the estimated parameter h_2 its measurement sensitivity is evaluated as [12]:

$$\Delta h_2 = \sqrt{2(P_x)_{h_2}} \cdot \Delta h, \quad (8)$$

with $(P_x)_{h_2}$ being the h_2 matrix element within P_x , and the altimetry measurement uncertainty Δh as defined in Eq. (6).

4.2. Estimated parameters

To single out the added value of including altimetry crossovers for POD, this work treats two distinctive scenarios:

- JUICE’s POD using Doppler measurements only
- JUICE’s POD using both Doppler and crossover measurements

Within both scenarios the exact same simulation settings are used, with both scenarios estimating the same parameters at the same epochs. To facilitate our primary goal, the study of the relative contribution of crossover data for orbit and parameter estimation, we have chosen to consider a reduced, but representative, set of estimation parameters:

- JUICE’s state,
- JUICE’s accelerometer biases as global parameter,
- Ganymede’s gravity field up to degree and order 12,
- Ganymede’s Love number k_2 ,

with only JUICE’s state being an arc-wise parameter, estimated daily over the simulation period of 160 days. This simulation period equals the length of the GCO500 mission phase as per CReMA 3.0. Our list of parameters differs from that considered by [9], who study in detail the performance of the 3GM instrument. Accelerometer biases are estimated as a global parameter under the assumption that JUICE’s accelerometer is turned on continuously throughout the analysed mission phase. For the gravity field we only consider the coefficients up to degree and order 12 (equal to the requirements of the JUICE missions), as crossovers’ influence onto high-degree coefficient estimation is expected (and corroborated in Section 6) to be small. For the estimation of JUICE’s state the used a priori covariances are 1 km for position and 1 m/s for velocity, for accelerometer biases they are 10^{-5} m/s². The estimation of the Love number h_2 is treated as an additional case to maintain comparability between the main scenarios, as this parameter cannot be estimated using Doppler data only.

5. Crossover partial derivatives

In this section we present the mathematical framework for the inclusion of altimetry crossover measurements into an orbit determination scheme. Specifically, the crossover partial derivatives are elaborated upon which are necessary to predict changes in their measurements from changes at the linearisation points through the design matrix H .

As shown in Eq. (1), a crossover observable describes the measurement difference at the crossing between two altimetry swaths over the same location on the surface. For the general description of our algorithm, we focus on the description of crossover sensitivity to changes in spacecraft state. Changes in the footprint coordinates due to variability of the central body (Ganymede) itself, due to effects such as tidal deformation are considered by the modelling of the tidal potential (k_2) and the estimation of the Love number h_2 . As discussed in Section 4.2, the estimation of h_2 is treated as an additional case to maintain comparability between results with and without crossovers.

As shown in Eq. (9), at the crossover point Ganymede’s static topography T can also be discarded as it is, by definition of a crossover, the same for both arcs:

$$h_{\otimes} = h_{\otimes 2} - h_{\otimes 1} = (r_2 - T) - (r_1 - T) = r_2 - r_1, \quad (9)$$

with r_1 and r_2 being JUICE’s radial distance to Ganymede’s centre of mass at the first and second arc, respectively. To calculate the required crossover measurement partial derivatives, Eq. (1) is rewritten as:

$$h_{\otimes}(r(t_1), r(t_2)) = |r(t_2)| - |r(t_1)| = |r_2| - |r_1|. \quad (10)$$

For Eq. (10) to be applicable the following condition must be satisfied:

$$\hat{r}^B(t_1) = \hat{r}^B(t_2), \quad (11)$$

with \hat{r} being the unit vector of the position vector r and the superscript B indicating that the vector is expressed in the body-fixed frame of Ganymede. The condition described in Eq. (11) ensures that both crossovers arc-components (at t_1 and t_2) occur at the same longitude and latitude of the body B . The underlying assumption behind this method is that the spacecraft is purely nadir-pointing during altimetry measurement periods. We discuss the influence of this assumption on our method in general, and our work specifically, at the end of this section. In short, the assumption limits the direct applicability of the method to simulation studies. The incorporation of pointing error into the model will require the consideration of additional terms in our governing equations.

To a first approximation, the partial derivative of a crossover observable w.r.t. the change in the initial state vector of arc i , denoted $s((t_0)_i)$ of the spacecraft can be described as:

$$\frac{\partial h_{\otimes}(t)}{\partial s((t_0)_i)} = \frac{\partial h_{\otimes}}{\partial s(t_1)} \frac{\partial s(t_1)}{\partial s((t_0)_i)} + \frac{\partial h_{\otimes}}{\partial s(t_2)} \frac{\partial s(t_2)}{\partial s((t_0)_i)}, \quad (12)$$

where $(t_0)_i$ is the initial epoch of the i th arc over which the spacecraft state is to be estimated. The crossovers will have non-zero partial derivatives to two initial states $s(t_0)_i$ (if t_2 and t_1 fall in different arcs) or a single non-zero derivative if both crossover times fall in the same arc. In what follows we will, without loss of generality, present the formulation for a single t_0 , omitting the i subscript.

The change in a later state vector $s(t_1)$ due to a change in the initial state $s(t_0)$ is calculated by making use of the conventional *state transition matrix*. As shown in Eq. (10), a crossover measurement is only explicitly dependent on the spacecraft position, not on the spacecraft velocity, making it possible to reduce Eq. (12) to:

$$\frac{\partial h_{\otimes}}{\partial s(t_0)} = \frac{\partial h_{\otimes}}{\partial r(t_1)} \frac{\partial r(t_1)}{\partial s(t_0)} + \frac{\partial h_{\otimes}}{\partial r(t_2)} \frac{\partial r(t_2)}{\partial s(t_0)}. \quad (13)$$

Importantly, the crossover times t_1 and t_2 in Eq. (12) do not need to occur in the same arc, dramatically increasing the number of available

crossover points for estimation. Evaluating Eq. (13) using Eq. (10) for h_{\otimes} yields:

$$\frac{\partial h_{\otimes}}{\partial s(t_0)} = -\frac{\partial |r(t_1)|}{\partial r(t_1)} \frac{\partial r(t_1)}{\partial s(t_0)} + \frac{\partial |r(t_2)|}{\partial r(t_2)} \frac{\partial r(t_2)}{\partial s(t_0)}. \quad (14)$$

We have tested the model of Eq. (14), by comparing the analysis' partial derivatives it produced with numerical partial derivatives. Unfortunately, we find that the results obtained by this first approximation do not capture the majority of the sensitivity of crossovers to spacecraft state, with errors of the derivatives averaged over a single arc in the range of $\gtrsim 100\%$ for most state elements (results for a single representative estimation arc are shown in Table 1). These results are discussed in more details later in this section.

For a more detailed linearised model for sensitivity of crossover observable to initial state, the changes in the crossover location, and thus also changes in the crossover times t_1 and t_2 , have to be incorporated. These are obtained by first rewriting Eq. (1) as:

$$h_{\otimes}(r_1, r_2, t_1, t_2) = |r_2(t_2(r_1, r_2))| - |r_1(t_1(r_1, r_2))|. \quad (15)$$

This expression takes into account the crossover times t_1 and t_2 , which heavily depend on the crossover location at $\hat{r}^B(t_1) = \hat{r}^B(t_2)$. Using Eq. (15) the crossover partial derivative w.r.t. its current position vector r_1 is:

$$\frac{\partial h_{\otimes}}{\partial r_1} = \frac{\partial |r_2|}{\partial t_2} \frac{\partial t_2}{\partial r_1} - \frac{\partial |r_1|}{\partial r_1} - \frac{\partial |r_1|}{\partial t_1} \frac{\partial t_1}{\partial r_1}. \quad (16)$$

The derivatives for the times t_1 and t_2 w.r.t. r_1 are

$$\frac{\partial t_2}{\partial r_1} = \frac{\partial t_2}{\partial r_1^B} \frac{\partial r_1^B}{\partial r_1}, \quad (17)$$

$$\frac{\partial t_1}{\partial r_1} = \frac{\partial t_1}{\partial r_1^B} \frac{\partial r_1^B}{\partial r_1}. \quad (18)$$

Of the terms above, the following can be obtained directly:

$$\frac{\partial |r_2|}{\partial t_2} = v_2 \cdot \hat{r}_2 \quad ; \quad \frac{\partial |r_1|}{\partial t_1} = v_1 \cdot \hat{r}_1, \quad (19)$$

$$\frac{\partial |r_2|}{\partial r_2} = (\hat{r}_2)^T, \quad (20)$$

$$\frac{\partial r_1^B}{\partial r_1} = R^{B/I}(t_1) \quad ; \quad \frac{\partial r_2^B}{\partial r_2} = R^{B/I}(t_2), \quad (21)$$

with $R^{B/I}(t)$ being the rotation matrix from the inertial frame to the body-fixed frame at time t . Now, only the terms $\partial t_2/\partial r_1^B$ and $\partial t_1/\partial r_1^B$ must be defined. To define the independent elements of this derivative (derivatives w.r.t. x_1^B, y_1^B, z_1^B), three conditions are defined below and depicted in Fig. 3.

- Any change in radial direction $\hat{r}_1^B = \hat{r}_2^B$ has no effect on either t_1 or t_2 , as the condition presented in Eq. (11) remains unaffected. Therein, only the magnitude of the crossover measurement is affected, while the crossover location remains the same.

$$\frac{\partial t_2}{\partial r_1^B} \cdot \hat{r}_1^B = 0. \quad (22)$$

- Any change of r_1^B in the direction of \hat{v}_1^B has no effect on the crossover time t_2 , as the crossover point on the arc of t_2 remains the same, while only inducing a change in t_1 :

$$\frac{\partial t_2}{\partial r_1^B} \cdot \hat{v}_1^B = 0. \quad (23)$$

- Lastly, a change of r_1^B in the direction of \hat{v}_2^B induces a change in t_2 . This change in t_2 is directly proportional to the magnitude of the horizontal component of $\hat{v}_2^B = |\hat{v}_{2,H}^B|$ which gives the time/distance from a given measurement to the crossover itself. Hereby no changes are introduced to t_1

$$\frac{\partial t_2}{\partial r_1^B} \cdot \hat{v}_2^B = \frac{1}{|\hat{v}_{2,H}^B|}. \quad (24)$$

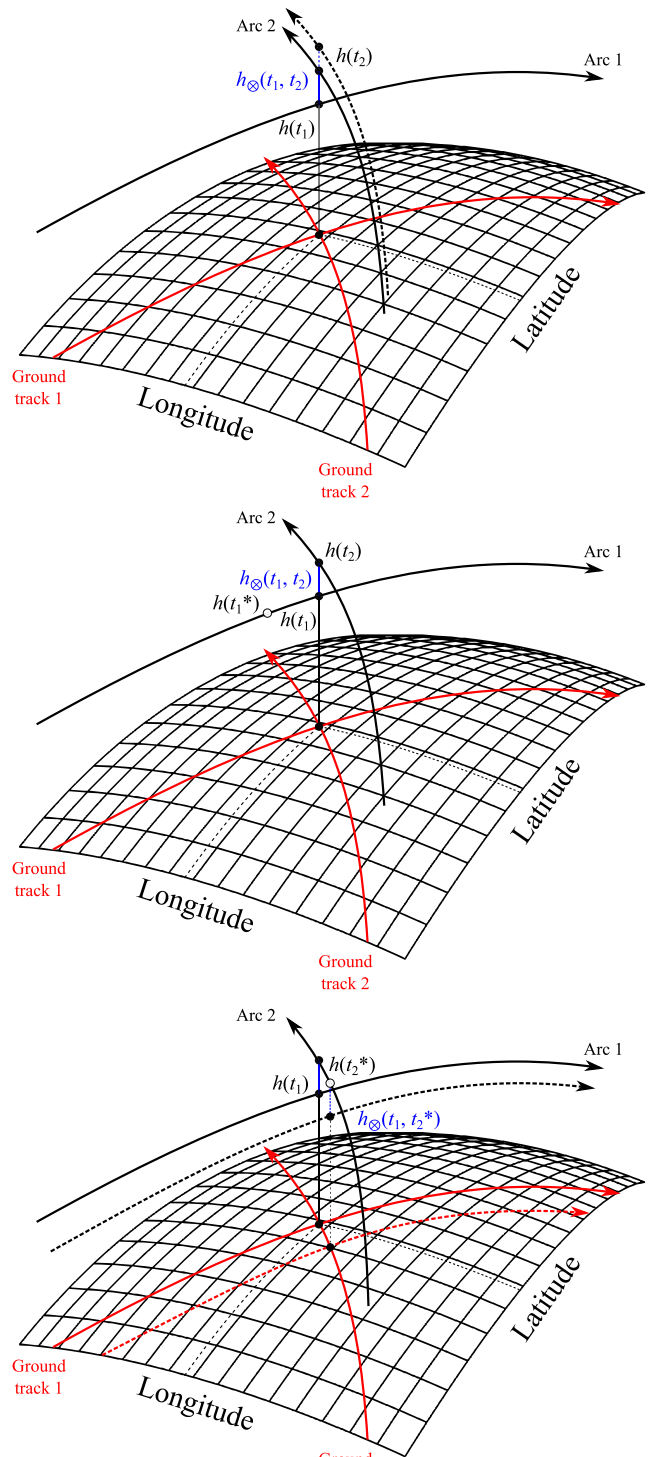


Fig. 3. Depiction of a change of crossover measurement in radial direction (top, Eq. (22)), in the direction of \hat{v}_1^B (middle, Eq. (23)) and in the direction of \hat{v}_2^B (bottom, Eq. (24)).

The horizontal component of \hat{v}_2^B is obtained via subtracting its radial velocity component

$$\hat{v}_{2,H}^B = \hat{v}_2^B - \hat{v}_2^B \cdot \hat{r}_2^B. \quad (25)$$

The conditions detailed in Eq. (22), Eq. (23) and Eq. (24) can be summarised as

$$A_{t_2r_1} \cdot \frac{\partial t_2}{\partial \mathbf{r}_1^B} = \mathbf{b}_{t_2r_1} \quad (26)$$

$$\text{with } A_{t_2r_1} = \left((\hat{\mathbf{r}}_2^B)^T, (\hat{\mathbf{v}}_1^B)^T, (\hat{\mathbf{v}}_2^B)^T \right) \quad \text{and} \quad \mathbf{b}_{t_2r_1} = \left(0, 0, |\hat{\mathbf{v}}_{2,H}^B|^{-1} \right)^T \quad (27)$$

By inverting this linear equation we obtain the needed partial derivatives

$$\frac{\partial t_2}{\partial \mathbf{r}_1^B} = A_{t_2r_1}^{-1} \mathbf{b}_{t_2r_1} \quad (28)$$

Equally, the three independent elements of \mathbf{r}_1^B for $\partial t_1 / \partial \mathbf{r}_1^B$ can be constrained with the following conditions:

$$\frac{\partial t_1}{\partial \mathbf{r}_1^B} \cdot \hat{\mathbf{r}}_1^B = 0 \quad ; \quad (29)$$

$$\frac{\partial t_1}{\partial \mathbf{r}_1^B} \cdot \hat{\mathbf{v}}_2^B = 0 \quad (30)$$

$$\frac{\partial t_1}{\partial \mathbf{r}_1^B} \cdot \hat{\mathbf{v}}_1^B = -|\hat{\mathbf{v}}_{1,H}^B|^{-1} \quad (31)$$

Contrary to Eq. (24), if \mathbf{r}_1^B experiences a change in the direction in the in-plane direction of \mathbf{v}_1^B , i.e. along its own arc, the new crossover location will occur earlier in time. Therein, t_2 experiences no changes while t_1 becomes smaller, resulting in a negative derivative as shown in Eq. (31). These conditions lead to

$$\frac{\partial t_2}{\partial \mathbf{r}_1^B} = A_{t_1r_1}^{-1} \mathbf{b}_{t_1r_1} \quad (32)$$

$$\text{with } A_{t_1r_1} = \left((\hat{\mathbf{r}}_1^B)^T, (\hat{\mathbf{v}}_2^B)^T, (\hat{\mathbf{v}}_1^B)^T \right) \quad \text{and} \quad \mathbf{b}_{t_1r_1} = \left(0, 0, -|\hat{\mathbf{v}}_{1,H}^B|^{-1} \right)^T \quad (33)$$

Making use of the equations above, Eq. (16) can be rewritten as:

$$\frac{\partial h_\otimes}{\partial \mathbf{r}_1} = \frac{\partial |r_2|}{\partial t_2} \left(\frac{\partial t_2}{\partial \mathbf{r}_1^B} \frac{\partial \mathbf{r}_1^B}{\partial \mathbf{r}_1} \right) - \frac{\partial |r_1|}{\partial \mathbf{r}_1} - \frac{\partial |r_1|}{\partial t_1} \left(\frac{\partial t_1}{\partial \mathbf{r}_1^B} \frac{\partial \mathbf{r}_1^B}{\partial \mathbf{r}_1} \right), \quad (34)$$

$$= (\mathbf{v}_2 \cdot \hat{\mathbf{r}}_2) \cdot ((A_{t_2r_1}^{-1} \cdot \mathbf{b}_{t_2r_1}) \cdot \mathbf{R}^{B/I}(t_2)) \hat{\mathbf{r}}_1^T - \hat{\mathbf{r}}_1^T - (\mathbf{v}_1 \cdot \hat{\mathbf{r}}_1) \cdot ((A_{t_1r_1}^{-1} \cdot \mathbf{b}_{t_1r_1}) \cdot \mathbf{R}^{B/I}(t_1)). \quad (35)$$

Equally, the partial derivative of the crossover observable w.r.t. a change in \mathbf{r}_2 is obtained symmetrically yielding:

$$\frac{\partial h_\otimes}{\partial \mathbf{r}_2} = \frac{\partial |r_2|}{\partial \mathbf{r}_2} + \frac{\partial |r_2|}{\partial t_2} \left(\frac{\partial t_2}{\partial \mathbf{r}_2^B} \frac{\partial \mathbf{r}_2^B}{\partial \mathbf{r}_2} \right) - \frac{\partial |r_1|}{\partial t_1} \left(\frac{\partial t_1}{\partial \mathbf{r}_2^B} \frac{\partial \mathbf{r}_2^B}{\partial \mathbf{r}_2} \right), \quad (36)$$

$$= \hat{\mathbf{r}}_2^T + (\mathbf{v}_2 \cdot \hat{\mathbf{r}}_2) \cdot ((A_{t_2r_2}^{-1} \cdot \mathbf{b}_{t_2r_2}) \cdot \mathbf{R}^{B/I}(t_2)) - (\mathbf{v}_1 \cdot \hat{\mathbf{r}}_1) \cdot ((A_{t_1r_2}^{-1} \cdot \mathbf{b}_{t_1r_2}) \cdot \mathbf{R}^{B/I}(t_1)), \quad (37)$$

$$\text{with } A_{t_2r_2} = \left((\hat{\mathbf{r}}_2^B)^T, (\hat{\mathbf{v}}_1^B)^T, (\hat{\mathbf{v}}_2^B)^T \right), \quad \mathbf{b}_{t_2r_2} = \left(0, 0, -|\hat{\mathbf{v}}_{2,H}^B|^{-1} \right), \quad (38)$$

$$A_{t_1r_2} = \left((\hat{\mathbf{r}}_1^B)^T, (\hat{\mathbf{v}}_2^B)^T, (\hat{\mathbf{v}}_1^B)^T \right) \quad \text{and} \quad \mathbf{b}_{t_1r_2} = \left(0, 0, |\hat{\mathbf{v}}_{1,H}^B|^{-1} \right). \quad (39)$$

These expressions describe the change of a crossover measurement due to a change in either \mathbf{r}_1 or \mathbf{r}_2 . Only by using these more detailed partial derivatives is it possible to include crossover measurements into the design matrix H and to make use of altimetry crossovers for orbit determination.

To evaluate the validity of the crossover partial derivatives, we have compared our results from these analytical formulations to numerically obtained partial derivatives. Table 1 shows the average error of the crossover partial derivatives when using Eq. (14), referred to as *Basic*, and the more detailed expressions for $\partial h_\otimes / \partial \mathbf{r}_1$ and $\partial h_\otimes / \partial \mathbf{r}_2$ derived above, referred to as *Detailed*. This table shows the results for a single representative estimation arc. While the specific numbers are different for other arcs, their order of magnitude is not. The *Basic* derivatives'

Table 1

Average relative difference for *Basic*, from Eq. (14) and *Detailed*, incorporating Eqs. (16) and (37), analytical crossover measurement partial derivatives with respect to numerical partial derivatives. These results are averaged over a single representative estimation batch.

Average relative difference of analytical and numerical partials		
	<i>Basic</i> [%]	<i>Detailed</i> [%]
$\partial h_\otimes / \partial x_0$	47.593	0.265
$\partial h_\otimes / \partial y_0$	283.902	0.229
$\partial h_\otimes / \partial z_0$	556.824	0.419
$\partial h_\otimes / \partial v_{x,0}$	1357.759	1.608
$\partial h_\otimes / \partial v_{y,0}$	443.710	0.378
$\partial h_\otimes / \partial v_{z,0}$	152.499	0.139

inability to accurately calculate changes in crossover measurements originates in their failure to address changes in crossover locations. Instead, they only focus on the radial orbit changes over a location where the evaluated crossover can no longer be found. Due to the large discrepancy between the results of numerically obtained partial derivatives and those obtained with Eq. (14), any analysis which relies on this first approximation should be regarded critically. Finally, we note that the remaining differences between our analytical and numerical partials for the *Detailed* model (here ~ 1%) largely stem from numerical errors: We have used a simple central-difference method to compute the numerical partials, for which we have not fully optimised the time step used.

An important limitation of the method we present here is the fundamental assumption that Eq. (9) is valid: Nadir-pointing is assumed. In reality, this assumption will not hold exactly, for which three aspects need to be considered. Firstly, the fact that the spacecraft's body-fixed latitude and longitude will not be exactly equal to the altimetry crossover location will require additional terms to be incorporated into our formulation. The absence of off-nadir pointing in our formulation means that the equations as given cannot be used directly for the analysis of crossover data as additional terms need to be added to incorporate this fact. The absence of exact nadir pointing does not influence the validity of Eqs. (16)–(21), none of which rely on the assumption in Eq. (11). However, the assumption does influence our manner of determining the conditions for $\partial t_2 / \partial (\mathbf{r}_1^B)$ and $\partial t_2 / \partial (\mathbf{r}_2^B)$. Specifically, the three conditions in Eqs. (22)–(24), and similarly (29)–(31), rely on the nadir assumption. One set of exceptions, where the influence of off-nadir pointing may be amplified, is when Eqs. (28) and (32) become close to singular. In those cases, even small off-nadir pointing angles may induce an error that is amplified to large changes in the crossover partial derivatives. However, in cases where the solution to either of these equations is close to ill-posed, the crossovers should be discarded in any event, as they would represent cases where the two tracks are close to parallel (or either track is vertical, which is a pathological case that will not be observed in reality).

Secondly, since the location of the crossovers is slightly mis-identified by omitting any off-nadir pointing in the model, the timing of the crossover will also be slightly in error. An off-nadir pointing of 10 arcseconds corresponds to a ~25 m offset between the spacecraft ground track and the altimetry swath, resulting in a crossover timing error of up to ~14 ms. Should the pointing vector be known, it is possible to account for it by shifting the epoch where the crossover is evaluated on each of both swaths. As with Eq. (23), for arc 2 only the along-track component of the crossover location shift has an effect in t_2 . Naturally, this applies equally to arc 1 and t_1 , Eq. (31). However, the major variations in the partial derivatives are expected to occur with a period on the order of the spacecraft's orbital period, and the very small partial derivative timing evaluation error (14 ms) will not unduly influence the results of our covariance analysis.

Thirdly, even if pointing is accounted for, as discussed in the previous point, pointing knowledge is not perfect with GALA having a nominal 1- σ pointing knowledge uncertainty of 10 arcseconds. At the

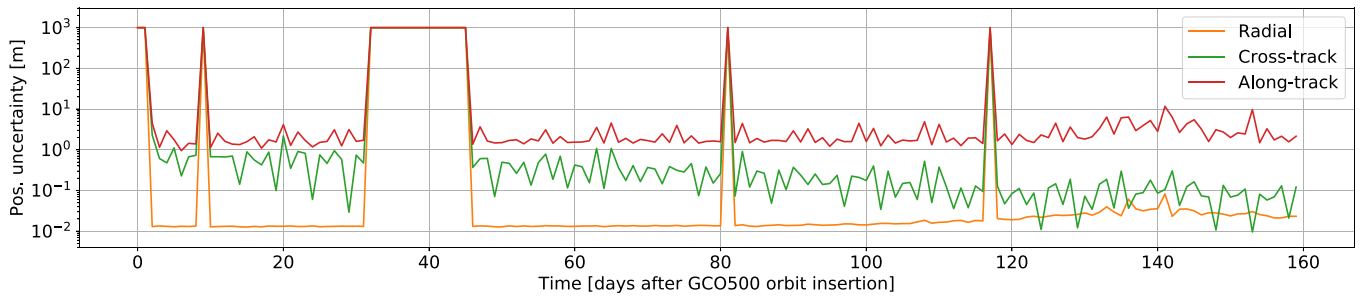


Fig. 4. Arc initial position uncertainty using Doppler data only.

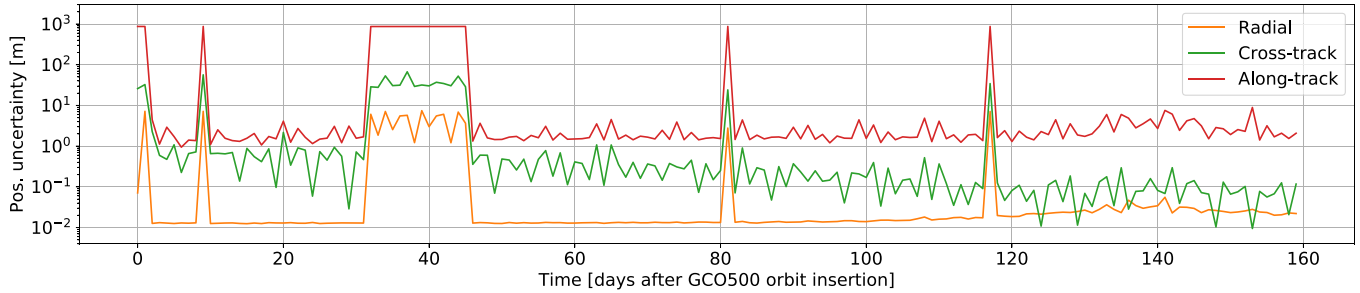


Fig. 5. Arc initial position uncertainty using both Doppler data and altimetry crossovers.

JUICE altitude of 500 km, this corresponds to an average measurement error of up to 2.18 m for each altimetry measurement (Eq. (3)). In our simulations, this pointing knowledge uncertainty is taken into account in the altimetry crossover error budget (Section 3.2) which determines the weighting of the crossover data, see Eq. (7).

As a result of the points raised above, our formulation technically is only valid for pure nadir pointing. For the case of JUICE, this assumption will very nearly hold throughout the mission, and the stated equations that are influenced by the nadir-pointing assumption all remain very nearly true, even when incorporating off-nadir pointing. Consequently, the formulation we provide here is adequate for a covariance analysis to predict the performance of the altimetry crossovers.

Finally, the derivatives w.r.t. h_2 are directly derived by computing the associated derivatives of T in Eq. (9) at the crossover times t_2 and t_1 . The influence of the libration amplitude (or any other rotational characteristic) on the term is obtained through following the same scheme as above (taking the direct derivatives, as well as the derivatives of the crossover times, w.r.t. rotational parameter), and evaluating the resulting partial derivatives of the rotation matrices $R^{B/I}$ w.r.t. rotational parameter at crossover times t_2 and t_1 . Thus, the crossover observables provide an additional approach for the measurement of the rotational state, which can be compared to estimates obtained from other methods [11].

6. Results

The presented results are the *formal* estimation errors of the POD scheme which are obtained from the covariance matrix of the estimated parameters P_x . These errors are denoted formal, since they represent the attainable errors under certain mathematical model assumptions, specifically the fact that all noise is Gaussian, unbiased and uncorrelated, and that simulation model and truth model of the dynamics are equal. Unfortunately, such a perfect recreation of JUICE's force environment is not feasible using actual measurements, resulting in estimation errors which must be regarded as too optimistic. Further details on the effects of remaining accelerometer noise on JUICE's orbit determination can be found in [9].

6.1. Doppler data only

Using 65,000 simulated Doppler measurements (see Section 3.1), we obtained the formal JUICE position uncertainties shown in Fig. 4. In this figure, the most prominent features are the five peaks in estimation uncertainty. These peaks are a direct result of periods with no available Doppler data. The large Doppler gap from day 32 until day 46 after GCO500 orbit insertion originates partly in an occultation by the Sun with Doppler measurements around it being discarded due to high plasma noise. It is worth mentioning that more recent JUICE trajectories (CR_{EMA}) do not encounter this occultation by the sun and are more beneficial for tracking, see Section 3. The minor occultations at days 0–2, 9, 81 and 117 are due to Jupiter occultations. In these cases, the postfit uncertainty reverts to the *a priori* information.

Another prominent feature of Fig. 4 is the degradation of the estimation uncertainty in radial direction, which even becomes temporarily worse than the estimation uncertainty in cross-track direction. This degradation is assigned to the orientation of JUICE's orbital plane as seen from Earth, shown as viewing angle in Fig. 6. The viewing angle represents the angle between a vector perpendicular to JUICE's orbital plane and the vector between Earth and Ganymede. As the viewing angle decreases, JUICE's orbit becomes close to perpendicular to Earth's line of sight. As a result, the Doppler measurements' sensitivity to the in-plane motion of the spacecraft is significantly reduced.

6.2. Inclusion of crossovers

When both Doppler and 631,000 crossover measurements are used for orbit determination, estimation uncertainties during periods without Doppler data drastically improve as can be seen in Fig. 5. This originates in the availability of measurements for every estimation arc. Although there are more crossover than Doppler measurements, crossovers do not have an overwhelming effect on the estimation results as crossovers have a substantially higher measurement uncertainty. For periods without Doppler data, including crossovers leads to average uncertainties of approx. 5 m radially, 36 m cross-track and 870 m along-track, as shown in Fig. 5. Due to our idealised simulation and noise environment, these are not specific numbers that we expect but

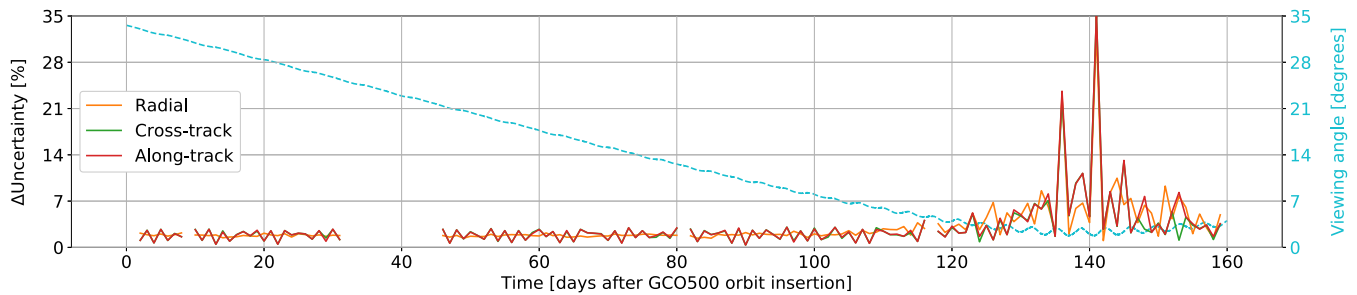


Fig. 6. Uncertainty improvement when crossover measurements are included.

rather magnitude ranges in estimation. For readability, Fig. 6 only shows uncertainty improvements for periods not afflicted by occultations which represents nominal POD cases. A noticeable feature of Fig. 6 is the large increase in uncertainty improvement towards the later estimation epochs. As with the degradation of state uncertainty discussed in Section 6.1, this estimation improvement originates in the viewing angle of JUICE's orbit from Earth. As Doppler measurements become less conclusive, the use of crossover measurements significantly aids in constraining JUICE's orbit. These uncertainty improvements towards later periods are further detailed in Table 2.

For periods without Doppler data, Fig. 5 and Table 2 both show that crossover measurements improve position uncertainty in radial direction the strongest, with uncertainty improvements in along-track direction being lowest. These improvements demonstrate that crossover altitude differences can effectively constrain the size and shape of a spacecraft orbit.

Moreover, the use of crossovers allows information from periods with tracking data to be transferred to periods without tracking data, if t_1 lies in an arc without Doppler data, and t_2 in a period with Doppler data (or vice versa). We point out that this situation, in which low-quality POD arcs benefit from high-quality POD arcs, represents an ideal situation. Achieving an optimal inclusion of crossovers will require a detailed analysis of the data sets, with careful weighting of the crossover data. Specifically, if the crossover data is 'overweighted' (e.g. noise properties are assessed too optimistically), the situation may become reversed, with the orbit quality for arcs with high-accuracy Doppler data being degraded by the incorporation of the crossover link to low-accuracy arcs. The orbit quality (quantified by e.g. arc overlaps) when incorporating the crossovers should be carefully assessed in this process, to ensure that no orbit degradation is introduced. In the present analysis, we omit this step, and interpret our results as being an idealised situation, consistent with our choice of covariance study as an analysis method.

For the estimation of global parameters, estimation improvements are consistently low as the estimation of global parameters uses measurements of *all* estimation arcs, leading to a much larger number of available Doppler measurements for their estimation. The uncertainties of accelerometer biases have magnitudes of 10^{-8} m/s² for the Doppler-only estimation, with the addition of crossover measurements lowering their uncertainty by 1.3% radially and 1.6% in cross-track and along-track direction. For the estimation of gravity field parameters uncertainty improvements of up to 11% are found for low-degree coefficients. However, uncertainty improvements rapidly decrease with an increase of the coefficients' degree resulting in improvements of less than 1% for harmonics of higher degree and order. The resulting average improvement for all gravity field coefficients is 0.8%. Similarly, the estimation improvement for the estimation of the Love number k_2 is 5.3%. No significant improvement in correlations between estimated parameters was found when crossover measurements are included.

Table 2

Position uncertainty improvement with altimetry crossovers.

	Average improvement in position uncertainty [%]					
	Radial		Cross-track		Along-track	
	avg.	max.	avg.	max.	avg.	max.
pre day 100	1.819	2.442	1.859	3.071	1.855	3.049
post day 100	4.885	32.64	4.334	35.218	4.628	35.347
total	3.03	32.64	2.895	35.218	3.016	35.347

6.3. Variation in parameters

In addition to our nominal estimation case described in Section 4.2, a number of additional cases was studied which employed different measurement uncertainties, estimation arc lengths, and sets of estimated parameters whose results are briefly presented. In such one case, the Love number h_2 is estimated as it cannot be estimated using Doppler data only. Using crossovers, we obtain an h_2 estimation uncertainty of 0.00153 which is expectedly lower than in previous studies due to the larger number of crossover measurements we employ [11,12].

In an additional case, a degraded Doppler precision of 5×10^{-5} m/s was used resulting in higher uncertainty improvements when crossover are included. Such a decrease in Doppler noise levels would be representative of missions that employ a single-frequency (X-band) tracking system, as opposed to the dual-frequency system employed by 3GM. The resulting average state estimation improvements are 42%, 56% and 56% in radial, cross and along-track direction during nominal estimation periods and up to 89%, 90% and 92% in radial, cross and along-track direction for periods with unfavourable Earth viewing angles. These results are expected as this work uses a *weighted* estimation scheme, see Section 4.

While not the expected case for JUICE, in another case the assumption was made that JUICE's accelerometer is not turned on continuously but only outside tracking periods. In this scenario it is necessary to estimate accelerometer biases after each accelerometer restart, resulting in an increase from 1129 to 1606 estimated parameters. We found that estimating accelerometer biases in an arc/wise fashion, instead of globally, leads to an increase in the crossover's contribution. However, For state estimation, the average improvements then become 21%, 5% and 5% for nominal estimation periods and 56%, 19% and 16% for periods with unfavourable Doppler data in radial, cross and along-track direction, respectively. For empirical accelerations, the average improvements become 9%, 20% and 9% for nominal estimation periods and 33%, 54% and 34% for periods with unfavourable Doppler data in radial, cross and along-track direction, respectively. While these results seem indicative of crossovers being a stronger contributor to local parameters, a wider variety of test cases need to be analysed to determine whether this is a general fact.

An increase in arc length, up to arcs consisting of 10 days, was found to decrease crossovers' uncertainty improvements, which originates from the larger number of Doppler measurements available for parameter estimation of a single arc. However, large estimation arcs

are unfeasible as measurement fitting will rapidly degrade until major factors have been sufficiently characterised such as JUICE's attitude, environment or WOL manoeuvres.

These findings show the benefits of including altimetry crossovers for a mission's POD, in particular when a degradation or absence of traditional tracking methods is encountered. Furthermore, if local parameters need to be estimated in addition to the spacecraft's state, crossovers provide an independent data set that can be useful in decoupling these additional local parameters from the spacecraft state. This characteristic is particularly valuable should accelerometer biases not be estimated as a global parameter (considered here) but as local parameters due to the necessity to switch accelerometers off and on during the GCO500 mission phase. While not treated here, previous studies have shown that the inclusion of crossover data can also improve pointing estimation [14,15,17].

7. Discussion

Consistent with previous studies [14,15,17], the results of this work show that crossover measurements can improve parameter estimation uncertainty. In particular, parameter uncertainty improvements due to crossovers become noticeably higher during periods with degradation or absence of Doppler measurements, such as during occultations or when the spacecraft orbital plane is perpendicular to Earth's line of sight, making crossover measurements particularly valuable for improved orbit estimation during such periods. Although spacecraft position knowledge during occultation periods (where only crossover measurements are available) is not as accurate as in periods where there is Doppler data, crossovers do provide orbit constraints in these periods. Furthermore, inter-arc crossovers uniquely allow information from Doppler data to be indirectly used to constrain the orbit during occultations, by transferring state knowledge between non-contiguous arcs.

The added value of crossovers also depends on the total number, and more specifically the type, of estimated parameters with crossover contribution being lower if accelerometer biases are estimated as a single parameter, instead of arc-wise. When these biases are estimated arc-wise, estimation improvements due to crossovers increase from under 5% in all directions to average 21% radially and 5% in cross and along-track direction. In our nominal case study, the assumption is made that accelerometers are on continuously and their bias can be estimated as a global parameter. For more comprehensive future studies a larger number of estimated local parameters may need to be included (accelerometer bias drift, wheel off-loading manoeuvres, etc.). While modifications in Doppler data quality (see Section 3.2), or an improved Doppler data analysis strategy, such as a constrained multi-arc estimation method [31], are expected to decrease the contribution of altimetry crossovers, their inclusion is nonetheless expected to aid in constraining orbit reconstruction and parameter estimation. Further improvements are expected once our method is extended to account for off-nadir pointing and the estimation of the rotational state of the orbited body is included. Crucially, our method allows itself to be extended to the estimation of the h_2 Love number. By combining the estimation of state and h_2 , this will allow for a fully consistent and realistic estimate of how state errors propagate into h_2 errors, providing a more robust uncertainty bound for this crucial parameter.

To effectively use crossovers for POD, global coverage is ideal with their quadratic increase with the number of orbit revolutions quickly resulting in more individual measurements than with conventional tracking methods. However, due to crossovers' inherently larger measurement uncertainty, even a much larger number of crossovers will not majorly alter estimation results due to the respective lower measurement weighting. As sufficient crossovers only become available after a certain number of available arcs, they cannot be reliably used for orbit estimation during early JUICE missing phases. Limit cases for which the inclusion of crossovers is not recommended are truly

polar, or equatorial orbits, where the definition of crossovers becomes degenerate.

The inclusion of crossovers is computationally intensive as their determination requires checking all individual ground tracks for crossings with other arcs. Larger computational efforts of up to a tenfold were also noted during estimation, due to the exceptionally high number of available crossover measurements as their number grows quadratically with the number of orbit revolutions [15]. Additionally, estimation design matrix setup may be complicated, as a single observation can be sensitive to local parameters that are separated in time by an arbitrary interval. This is distinct from typical observables (e.g. Doppler), where a single observation is sensitive to local parameters in a single arc only. This can complicate the implementation of the model, and reduces the sparsity of the associated matrices.

For the effective use of crossovers for POD, necessary algorithm improvements include the use of a crossover tagging system to ensure that the same arcs are used for a given crossover measurement after each orbit adjustment. Iterative orbit adjustments can not only alter the chronological order of crossovers, they can also lead to crossover locations vanishing and new crossovers appearing. Naturally, additional computational loads also arise from crossover locations having to be recalculated after each iteration. To lessen these loads, it is recommended to use previous crossover locations as *a priori* information. Performing a representative test using a subset of only 5,900 crossover measurements, it was observed that the variation in the total number of crossovers was ~5%, which shows that neglecting such a tagging system can heavily impair estimation convergence due to crossover measurement mismatches between estimation iterations.

An additional challenge that is likely to come up in the practical application of our method is a correct data weighting scheme for the multiple data types. For instance, separate crossover observables will have errors that are unlikely to be truly independent. This fact can be incorporated into our scheme by applying a crossover weighting matrix that is non-diagonal, and will require meticulous analysis of the crossover data properties. Similarly, the uncertainty in the crossover data is unlikely to have a (near) perfectly Gaussian distribution with zero mean. This may be in part corrected for by the inclusion of observation biases and/or data pre-processing. We do note, however, that these aspects will reduce the influence of the crossover observables, compared to our analysis given here (as discussed in Section 6.2).

Unlike previous works [14,15,17], the use of crossovers presented here does not discriminate measurements depending on the ground intersection angle between ground tracks. The dependency is directly incorporated into our definition of the partial derivatives. We do point out however, that independently of the estimation method used such locations are highly sensitive to changes at the linearisation points, potentially leading to large changes in the crossover location. When using actual data, it is necessary to discard problematic crossover measurements as they might negatively impact convergence. Altimetry measurements with large pointing uncertainty should be discarded due to their inherent uncertainty on any respective crossover locations. Also, large measurement uncertainties over unfavourable surface slopes might lead to unaccounted, rapid changes in topography which is particularly critical should the pointing uncertainty lead to altimetry arc shifts larger than the altimetry footprint radius.

Another critical characteristic of laser altimetry measurements is their spacing between consecutive footprints. If measured over sloped terrain, the necessary interpolation of the topography at the crossover location can rapidly lead to a large error contribution. Known off-nadir pointing can be accounted for by respective epoch shifts on both arcs making up a crossover. Since our method is obtained using nadir pointing assumption, for its use measurements with large off-nadir pointing should nevertheless also be discarded as the respective partials are still missing in our formulations. The uncertainty of altimetry crossover locations depends both on spacecraft location uncertainty and pointing uncertainty. Here, the in-plane spacecraft uncertainty has a

magnitude of ~ 2 m while pointing uncertainty results in an arc shift of up to ~ 25 m. This difference in magnitude further emphasises the need of further efforts to enable pointing estimation when using crossovers.

Lastly, since the partial derivatives for the two interpolated altimetry measurements which make up one crossover measurement are independent from one another and only depend on the respective linearisation point for estimation, altimetry crossovers can be used on a multitude of spacecraft over the same body. This could be especially advantageous for missions made up of several spacecraft around highly unconstrained bodies. However, combining such data from multiple missions/spacecraft will require the calibration of the different instruments on different spacecraft to be critically assessed and compared, to prevent measurement biases from being introduced into the crossover observations.

8. Conclusion

This paper presents a mathematical formulation to include crossover measurements into orbit determination in detail, by using analytical partial derivatives under the assumption of nadir-pointing. It is shown that a simplified, first-order approximation is insufficient for the inclusion of crossovers into orbit determination procedures and that a more elaborate expression is required, which includes the change in crossover location due to changes in the crossover times t_1 and t_2 . The inclusion of crossover measurements is shown to improve spacecraft position only marginally ($\sim 1.8\%$) due to advancements in Doppler precision, with noticeable estimation improvements in case of Doppler data degradation or unavailability. Such cases occur if the spacecraft orbital plane become perpendicular to Earth's viewing vector or if they are viewing occultations. Additionally, the inclusion of crossovers allowed spacecraft state estimations for occultation periods with average uncertainties of 3 m, 30 m and 870 m in radial, cross and along-track direction, respectively. Uncertainty improvements are also attained for global parameters such as k_2 (5.3%), accelerometer biases ($\sim 1.5\%$) and spherical harmonics (0.8% in average, up to 11% for low-degree coefficients) with improvements rapidly decreasing for harmonics of increasing degree and order. Should accelerometer biases be estimated as local parameters, altimetry crossovers lead to larger average estimation improvements of 21% radially, and 5% in along and cross-track directions for state estimation and 9%, 20% and 9% in radial, cross and along-track direction for empirical accelerations.

Declaration of competing interest

The authors declare that they have no known competing financial interests or personal relationships that could have appeared to influence the work reported in this paper.

Acknowledgements

The authors thank Luciano Iess (Sapienza University of Rome), Claire Vallat (Operation Scientists for the JUICE mission), Arnaud Boutonnet (Mission Analyst for the JUICE mission) and four anonymous reviewers for their thoughtful comments. Part of this research was carried out within the framework of the DLR BigData Querschnittsplatform.

Appendix. Ganymede gravity field

See Table A.3.

Table A.3

Normalised Ganymede gravity field coefficients. n stands for degree, m for order, C for cosine coefficients and S for sine coefficients. Reference radius: 2634.0 km; μ : 9887.83445333 km³ s⁻². Values for coefficients up to degree and order 10 as in [26,29,38].

n	m	C	S
11	0	3.92×10^{-7}	0
11	1	2.94×10^{-7}	-4.55×10^{-7}
11	2	-9.04×10^{-8}	-7.50×10^{-8}
11	3	-2.75×10^{-7}	1.26×10^{-7}
11	4	1.28×10^{-8}	4.70×10^{-7}
11	5	-1.08×10^{-7}	5.31×10^{-7}
11	6	3.23×10^{-7}	-2.62×10^{-8}
11	7	-2.24×10^{-7}	4.16×10^{-7}
11	8	-2.66×10^{-8}	-2.73×10^{-7}
11	9	9.49×10^{-8}	3.47×10^{-7}
11	10	4.65×10^{-7}	5.55×10^{-8}
11	11	5.34×10^{-9}	-5.53×10^{-7}
12	0	-2.09×10^{-7}	0
12	1	2.45×10^{-7}	2.10×10^{-7}
12	2	1.13×10^{-7}	-9.68×10^{-8}
12	3	-2.39×10^{-7}	3.11×10^{-7}
12	4	3.92×10^{-7}	1.61×10^{-7}
12	5	4.62×10^{-7}	-4.77×10^{-7}
12	6	2.97×10^{-7}	-6.14×10^{-9}
12	7	3.85×10^{-7}	3.52×10^{-7}
12	8	-1.82×10^{-7}	-2.45×10^{-7}
12	9	2.20×10^{-7}	-1.67×10^{-7}
12	10	3.82×10^{-7}	3.54×10^{-7}
12	11	1.76×10^{-7}	-2.96×10^{-7}
12	12	-2.67×10^{-8}	6.46×10^{-8}

References

- [1] O. Grasset, M. Dougherty, A. Coustenis, E. Bunce, C. Erd, D. Titov, M. Blanc, A. Coates, P. Drossart, L. Fletcher, H. Hussmann, R. Jaumann, N. Krupp, J.-P. Lebreton, O. Prieto-Ballesteros, P. Tortora, F. Tosi, T.V. Hoolst, JUPITER ICY moons explorer (JUICE): An ESA mission to orbit Ganymede and to characterise the Jupiter system, *Planet. Space Sci.* 78 (2013) 1–21, <http://dx.doi.org/10.1016/j.pss.2012.12.002>.
- [2] F. Bagenal, T. Dowling, W. McKinnon, W. McKinnon, J. Bell, D. Jewitt, R. Lorenz, C. Murray, F. Nimmo, *Jupiter: The Planet, Satellites and Magnetosphere*, Cambridge University Press, 2004.
- [3] M.G. Kivelson, K.K. Khurana, C.T. Russell, R.J. Walker, J. Warnecke, F.V. Coroniti, C. Polanskey, D.J. Southwood, G. Schubert, Discovery of Ganymede's magnetic field by the Galileo spacecraft, *Nature* 384 (1996) 537–541, <http://dx.doi.org/10.1038/384537a0>.
- [4] M. Kivelson, K. Khurana, M. Volwerk, The permanent and inductive magnetic moments of Ganymede, *Icarus* 157 (2) (2002) 507–522, <http://dx.doi.org/10.1006/icar.2002.6834>.
- [5] H.B. Niemann, S.K. Atreya, G.R. Carignan, T.M. Donahue, J.A. Haberman, D.N. Harpold, R.E. Hartle, D.M. Hunten, W.T. Kasprzak, P.R. Mahaffy, T.C. Owen, S.H. Way, The composition of the Jovian atmosphere as determined by the Galileo probe mass spectrometer, *J. Geophys. Res.: Planets* 103 (E10) (1998) 22831–22845, <http://dx.doi.org/10.1029/98JE01050>.
- [6] B. Ragent, D.S. Colburn, K.A. Rages, T.C.D. Knight, P. Avrin, G.S. Orton, P.A. Yanamandra-Fisher, G.W. Grams, The clouds of Jupiter: Results of the Galileo Jupiter mission probe nephelometer experiment, *J. Geophys. Res.: Planets* 103 (E10) (1998) 22891–22909, <http://dx.doi.org/10.1029/98JE00353>.
- [7] C. Zimmer, K.K. Khurana, M.G. Kivelson, Subsurface oceans on Europa and Callisto: Constraints from Galileo magnetometer observations, *Icarus* 147 (2) (2000) 329–347, <http://dx.doi.org/10.1006/icar.2000.6456>.
- [8] T. Spohn, G. Schubert, Oceans in the icy Galilean satellites of Jupiter? *Icarus* 161 (2) (2003) 456–467, [http://dx.doi.org/10.1016/S0019-1035\(02\)00048-9](http://dx.doi.org/10.1016/S0019-1035(02)00048-9).
- [9] P. Cappuccio, A. Hickey, D. Durante, M.D. Benedetto, L. Iess, C. Plainaki, A. Milillo, A. Mura, Ganymede's gravity, tides and rotational state from JUICE's 3GM experiment simulation, *Planet. Space Sci.* (2020) 104902, <http://dx.doi.org/10.1016/j.pss.2020.104902>.
- [10] H. Hussmann, K. Lingenauber, R. Kallenbach, K. Enya, N. Thomas, L.M. Lara, C. Althaus, H. Araki, T. Behnke, J.M. Castro-Marin, H. Eisenmenger, T. Gerber, M. Herranz de la Revilla, C. Hüttig, K. Ishibashi, J. Jiménez-Ortega, J. Kimura, M. Kobayashi, H.-G. Lötze, A. Lichopoj, F. Lüdicke, I. Martí nez Navajas, H. Michaelis, N. Namiki, H. Noda, J. Oberst, S. Oshigami, J.P. Rodríguez García, J. Rodrigo, K. Rösner, A. Stark, G. Steinbrügge, P. Thabaut, S. del Togno, K. Touhara, S. Villamil, B. Wendler, K. Wickhusen, K. Willner, The Ganymede laser altimeter (GALA): key objectives, instrument design, and performance, *CEAS*

- Space J. 11 (4) (2019) 381–390, <http://dx.doi.org/10.1007/s12567-019-00282-8>.
- [11] G. Steinbrügge, T. Steinke, R. Thor, A. Stark, H. Hussmann, Measuring Ganymede's librations with laser altimetry, *Geosciences* 9 (7) (2019) 320, <http://dx.doi.org/10.3390/geosciences9070320>.
- [12] G. Steinbrügge, A. Stark, H. Hussmann, F. Sohl, J. Oberst, Measuring tidal deformations by laser altimetry. A performance model for the Ganymede laser altimeter, *Planet. Space Sci.* 117 (2015) 184–191, <http://dx.doi.org/10.1016/j.pss.2015.06.013>.
- [13] E. Mazarico, M.K. Barker, G.A. Neumann, M.T. Zuber, D.E. Smith, Detection of the lunar body tide by the Lunar Orbiter Laser Altimeter, *Geophys. Res. Lett.* 41 (7) (2014) 2282–2288, <http://dx.doi.org/10.1002/2013GL059085>.
- [14] D.D. Rowlands, D.E. Pavlis, F.G. Lemoine, G.A. Neumann, S.B. Luthcke, The use of laser altimetry in the orbit and attitude determination of Mars Global Surveyor, *Geophys. Res. Lett.* 26 (9) (1999) 1191–1194, <http://dx.doi.org/10.1029/1999GL900223>.
- [15] G.A. Neumann, D.D. Rowlands, F.G. Lemoine, D.E. Smith, M.T. Zuber, Crossover analysis of Mars orbiter laser altimeter data, *J. Geophys. Res.: Planets* 106 (E10) (2001) 23753–23768, <http://dx.doi.org/10.1029/2000JE001381>.
- [16] D.D. Rowlands, F.G. Lemoine, D.S. Chinn, S.B. Luthcke, A simulation study of multi-beam altimetry for lunar reconnaissance orbiter and other planetary missions, *J. Geod.* 83 (8) (2008) 709, <http://dx.doi.org/10.1007/s00190-008-0285-y>.
- [17] E. Mazarico, D.D. Rowlands, G.A. Neumann, Orbit determination of the lunar reconnaissance orbiter, *J. Geod.* 86 (3) (2011) 193–207, <http://dx.doi.org/10.1007/s00190-011-0509-4>.
- [18] G. Steinbrügge, A. Stark, H. Hussmann, K. Wickhusen, J. Oberst, The performance of the BepiColombo Laser Altimeter (BELA) prior launch and prospects for mercury orbit operations, *Planet. Space Sci.* 159 (2018) 84–92, <http://dx.doi.org/10.1016/j.pss.2018.04.017>.
- [19] E. Mazarico, G.A. Neumann, D.D. Rowlands, D.E. Smith, Geodetic constraints from multi-beam laser altimeter crossovers, *J. Geod.* 84 (6) (2010) 343–354, <http://dx.doi.org/10.1007/s00190-010-0379-1>.
- [20] E. Mazarico, G.A. Neumann, M.K. Barker, S. Goossens, D.E. Smith, M.T. Zuber, Orbit determination of the lunar reconnaissance orbiter: Status after seven years, *Planet. Space Sci.* 162 (2018) 2–19, <http://dx.doi.org/10.1016/j.pss.2017.10.004>.
- [21] S.B. Luthcke, D.D. Rowlands, T.A. Williams, M. Sirota, Reduction of ice-sat systematic geolocation errors and the impact on ice sheet elevation change detection, *Geophys. Res. Lett.* 32 (21) (2005) <http://dx.doi.org/10.1029/2005GL023689>.
- [22] F.G. Lemoine, D.E. Smith, D.D. Rowlands, M.T. Zuber, G.A. Neumann, D.S. Chinn, D.E. Pavlis, An improved solution of the gravity field of mars (GMM-2B) from mars global surveyor, *J. Geophys. Res.: Planets* 106 (E10) (2001) 23359–23376, <http://dx.doi.org/10.1029/2000JE001426>.
- [23] TUDelft, TU Delft astrodynamics toolbox (TUDAT), 2019, 2019-06-01, <http://tudat.tudelft.nl/index.html>.
- [24] D. Dirx, L.I. Gurvits, V. Lainey, G. Lari, A. Milani, G. Cimò, T. Bocanegra-Bahamon, P. Visser, On the contribution of pride-juice to jovian system ephemerides, *Planet. Space Sci.* 147 (2017) 14–27.
- [25] D. Dirx, E. Mooij, B. Root, Propagation and estimation of the dynamical behaviour of gravitationally interacting rigid bodies, *Astrophys. Space Sci.* 364 (2019) 2, <http://dx.doi.org/10.1007/s10509-019-3521-4>.
- [26] ESOC, Consolidated Report on Mission Analysis (CReMA), Tech. Rep. 3.0, ESA, 2015, 2019-02-20, <https://www.cosmos.esa.int/web/spice/spice-for-juice>.
- [27] C.H. Acton, Ancillary data services of NASA's Navigation and Ancillary Information Facility, *Planet. Space Sci.* 44 (1) (1996) 65–70, [http://dx.doi.org/10.1016/0032-0633\(95\)00107-7](http://dx.doi.org/10.1016/0032-0633(95)00107-7).
- [28] C. Acton, N. Bachman, B. Semenov, E. Wright, A look towards the future in the handling of space science mission geometry, *Planet. Space Sci.* 150 (2018) 9–12, <http://dx.doi.org/10.1016/j.pss.2017.02.013>.
- [29] ESA, JUICE Definition Study Report (Red Book), Tech. Rep. 1.0, ESA, 2014.
- [30] D. Dirx, I. Prochazka, S. Bauer, P. Visser, R. Noomen, L.I. Gurvits, B. Vermeersen, Laser and radio tracking for planetary science missions - a comparison, *J. Geod.* 93 (2019) 2405–2420, <http://dx.doi.org/10.1007/s00190-018-1171-x>.
- [31] E.M. Alessi, S. Cicaló, A. Milani, G. Tommei, Desaturation manoeuvres and precise orbit determination for the BepiColombo mission, *Mon. Not. R. Astron. Soc.* 423 (3) (2012) 2270–2278, <http://dx.doi.org/10.1111/j.1365-2966.2012.21035.x>.
- [32] P. Cappuccio, V. Notaro, L. Iess, S. Asmar, J. Border, S. Ciarcia, A. Di Ruscio, E. Montagnon, J. De Vicente, M. Mercolino, M. Paik, L. Simone, F. Fiori, A. Palli, P. Tortora, M. Zannoni, J. Villalvilla, First results from cruise tests of the mercury orbiter radio science experiment (MORE) of ESA's BepiColombo mission, in: AGU Fall Meeting Abstracts, Vol. 2019, 2019, pp. P34A–04.
- [33] L. Iess, W.M. Folkner, D. Durante, M. Parisi, Y. Kaspi, Measurement of Jupiter's asymmetric gravity field, *Nature* 555 (8) (2018) 220–222, <http://dx.doi.org/10.1038/nature25776>.
- [34] L. Iess, M.D. Benedetto, N. James, M. Mercolino, L. Simone, P. Tortora, Astra: Interdisciplinary study on enhancement of the end-to-end accuracy for spacecraft tracking techniques, *Acta Astronaut.* 94 (2) (2014) 699–707, <http://dx.doi.org/10.1016/j.actaastro.2013.06.011>.
- [35] W.M. Folkner, L. Iess, J.D. Anderson, S.W. Asmar, Jupiter gravity field estimated from the first two Juno orbits, *Geophys. Res. Lett.* 44 (10) (2017) 4694–4700, <http://dx.doi.org/10.1002/2017GL073140>.
- [36] Y. Berquin, W. Kofman, A. Herique, G. Alberti, P. Beck, A study on Ganymede's surface topography: Perspectives for radar sounding, *Planet. Space Sci.* 77 (2013) 40–44, <http://dx.doi.org/10.1016/j.pss.2012.07.004>.
- [37] G. Steinbrügge, J.R.C. Voigt, D.M. Schroeder, A. Stark, M.S. Haynes, K.M. Scanlan, C.W. Hamilton, D.A. Young, H. Hussmann, C. Grima, D.D. Blankenship, The surface roughness of Europa derived from Galileo stereo images, *Icarus* 343 (2020) 113669, <http://dx.doi.org/10.1016/j.icarus.2020.113669>.
- [38] M. Boere, A. Boutonnet, Stationkeeping strategy for laplace-jgo science phase around ganymede, *Adv. Astronaut. Sci.* 142 (2012) 1867–1882.